

# INTERNATIONAL SOCIETY FOR SOIL MECHANICS AND GEOTECHNICAL ENGINEERING



*This paper was downloaded from the Online Library of the International Society for Soil Mechanics and Geotechnical Engineering (ISSMGE). The library is available here:*

<https://www.issmge.org/publications/online-library>

*This is an open-access database that archives thousands of papers published under the Auspices of the ISSMGE and maintained by the Innovation and Development Committee of ISSMGE.*

*The paper was published in the proceedings of the 7<sup>th</sup> International Conference on Earthquake Geotechnical Engineering and was edited by Francesco Silvestri, Nicola Moraci and Susanna Antonielli. The conference was held in Rome, Italy, 17 - 20 June 2019.*

## Calibration of a constitutive model for the cyclic loading responses of Fraser River Delta silt

R.W. Boulanger

*University of California, Davis, CA, USA*

D. Wijewickreme

*University of British Columbia, Vancouver, BC, Canada*

**ABSTRACT:** Calibration of the PM4Silt constitutive model for the cyclic loading responses of a natural deposit of Fraser River Delta silt is presented. The PM4Silt model is a stress-ratio controlled, critical state based, bounding surface plasticity model developed for representing clays and plastic silts in geotechnical earthquake engineering applications. The deposit of Fraser River Delta silt examined herein is a normally consolidated to lightly over-consolidated, low-plasticity silt (ML) with a plasticity index of about 4. Monotonic and cyclic undrained direct simple shear (DSS) tests were performed on normally consolidated, thin-walled tube samples. Calibration of the PM4Silt model was based on the monotonic and cyclic DSS test data, in-situ shear wave velocity measurements, and empirical relationships for strain-dependent secant shear moduli and equivalent damping ratios. The calibration process is described, and three alternative calibrations of the model are developed to illustrate the effect of emphasizing different behaviors during calibration. The results illustrate that PM4Silt is capable of reasonably approximating a range of monotonic and cyclic loading behaviors important to many earthquake engineering applications and is relatively easy to calibrate.

### 1 INTRODUCTION

Saturated, low-plasticity silts often exhibit cyclic loading responses that are intermediate in characteristics to the liquefaction behaviors associated with sand-like soils and cyclic softening behaviors associated with clay-like soils. These intermediate behaviors can be particularly challenging to represent constitutively in nonlinear dynamic analyses (NDAs), given that most constitutive models available for use in dynamic analysis programs have been developed specifically for sand-like or clay-like soils.

The PM4Silt plasticity model by Boulanger & Ziotopoulou (2018) was developed for representing clays and plastic silts in geotechnical earthquake engineering applications. The PM4Silt model builds on the framework of the stress-ratio controlled, critical state based, bounding surface plasticity PM4Sand model (version 3.1) described in Ziotopoulou & Boulanger (2016) and Boulanger & Ziotopoulou (2017). Modifications to the constitutive relationships, relative to PM4Sand, were designed to improve the model's ability to approximate key loading behaviors for clays and plastic silts, as opposed to those for purely nonplastic silts or sands. The key behaviors sought for most earthquake engineering applications are: (1) monotonic undrained shear strength; (2) cyclic undrained shear strength and associated stress-strain responses; and (3) secant shear moduli and equivalent damping ratios. The model was implemented as a dynamic link library for use with the finite difference program FLAC 8.0 (Itasca 2016).

This paper describes the calibration of the PM4Silt model for a natural deposit of Fraser River Delta (FRD) silt from Richmond, British Columbia. The deposit of FRD silt examined

is a normally consolidated to lightly over-consolidated, low-plasticity silt with a plasticity index (PI) of about 4. Monotonic and cyclic undrained direct simple shear (DSS) tests were performed on thin-walled tube samples. Calibration of the PM4Silt model was based on the monotonic and cyclic DSS test data, in-situ shear wave velocity measurements, and empirical relationships for strain-dependent secant shear moduli and equivalent damping ratios. The calibration process is described, and three alternative calibrations of the model are developed to illustrate the effect of emphasizing different behaviors during calibration. The simulation results illustrate that PM4Silt is capable of reasonably approximating a range of monotonic and cyclic undrained loading behaviors important to many earthquake engineering applications and is relatively easy to calibrate.

## 2 FRASER RIVER DELTA SILT

The subject site is located at the southern foot of a dyke along the north riverbank of the south arm of the Fraser River, near the intersection of Dyke Road and No. 3 Road in Richmond, British Columbia, Canada (Sanin & Wijewickreme 2006). This site is located in the Fraser River Delta (FRD) area, which extends approximately 23 km east-west and meets the sea over a length of about 40 km. The FRD deposits are Holocene in age and up to 300 m deep. The upper part of the delta topset unit is generally comprised of flood-plain silts and peat. The properties of FRD silts vary with location in the delta, but are generally soft and of low-plasticity.

The subsurface conditions at the site are shown in Figure 1, which includes data from a cone penetration test (CPT), a seismic dilatometer sounding, and mud-rotary boreholes with field vane shear tests (FVT). Surficial dyke fill materials extend to a depth of about 2 m, and are underlain by a deposit of silt with sand interlayers to a depth of about 19 m. Fixed piston tube samples of the silt were obtained from mud-rotary boreholes using specially fabricated 75-mm diameter, 0.9-m long tubes with no inside clearance, a five degree cutting edge, and 1.5 mm wall thickness. Samples from depths of 5.6 to 7.4 m were used for the advanced laboratory testing.

The silt was clayey to sandy with laminations at the mm scale, including thin interbeds of fine sand and silty sand, as illustrated by the photographs shown in Figure 2. Thicker interbeds of sand are also evident in the profiles of the CPT tip resistance ( $q_{tN} = q_t/P_A$ , where  $P_A =$  atmospheric pressure) and sleeve friction ratio ( $R_f$ ) in Figure 1. The silt was typically comprised of about 10% sand size, 80% silt size, and 10% clay size ( $< 2$  micron), and had a natural water content of about 34%, a liquid limit (LL) of about 30, a PI of about 4, and USCS classification of ML.

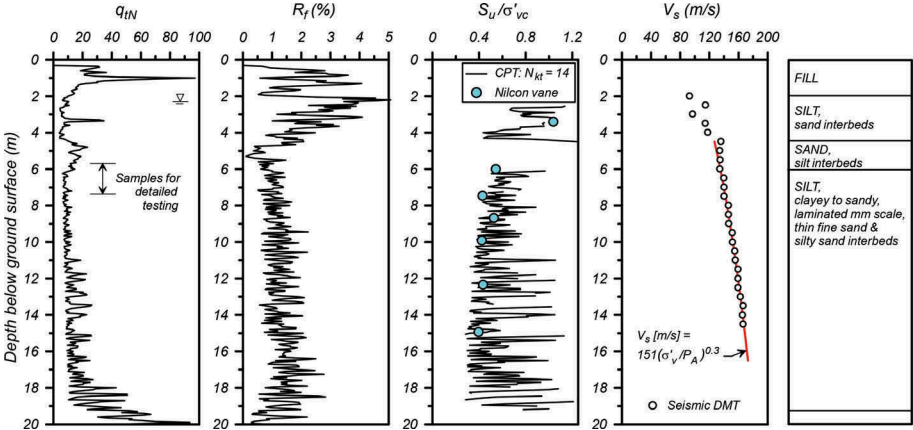


Figure 1. Soil profile and in-situ test data for the test site.

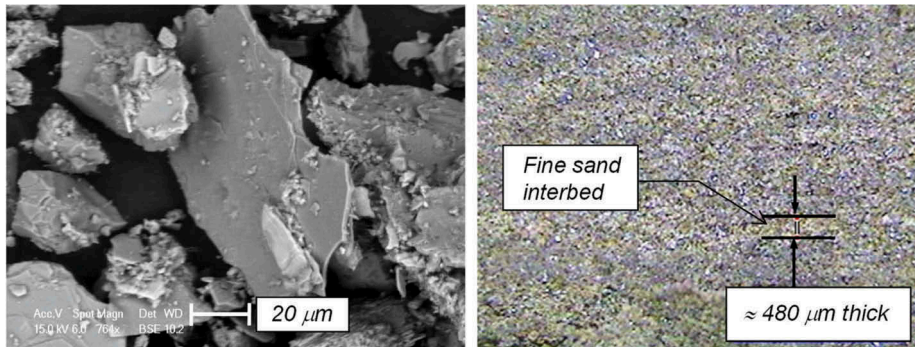


Figure 2. Images of Fraser River Delta silt: (a) microscopic view of silt particles, and (b) optical view of sub-millimeter fine sand interbeds within a silt specimen.

The silt deposit is normally consolidated to lightly over-consolidated over its full thickness based on interpretation of the consolidation tests, the in-situ test data, and the site's geologic history. The results of consolidation tests on samples from 5.6 to 7.4 m depth indicate over-consolidation ratios of about 1.0-1.2. The undrained shear strengths ( $s_u$ ) from the FVTs and CPT (based on  $N_{kt} = 14$ ) show the undrained shear strength ratios ( $s_u/\sigma'_{vc}$ ) decreasing slightly with increasing depth (Figure 1), which suggests that the silt becomes closer to normally consolidated at the larger depths. This interpretation of stress history is consistent with the known loading history of the site and expected effects of secondary compression.

The shear wave velocity ( $V_s$ ) in the silt ranges from about 135 m/s at 6 m depth to about 170 m/s at 16 m depth (Figure 1). The  $V_s$  in the silt increases in proportion to  $\sigma'_{vc}$  raised to a power of 0.3, which includes the effects of the slight decrease in void ratio with increasing confining stress in addition to the effects of increasing confining stress alone.

Series of monotonic and cyclic undrained (constant volume) DSS tests were performed on tube samples (Sanin & Wijewickreme 2006) and reconstituted specimens (Wijewickreme & Sanin 2008). The DSS tests were performed using an NGI-type device at the University of British Columbia. The DSS test specimens were trimmed to a diameter of 70 mm and height of 20-25 mm, placed inside a steel-wire reinforced membrane, and loaded under constant volume and height conditions. The cyclic DSS tests were performed under stress-controlled loading at a frequency of 0.1 Hz. Results of these tests are presented later in combination with the constitutive modeling results, but a few details warrant discussion at this point.

The  $s_u/\sigma'_{vc}$  ratios from the monotonic DSS tests range from 0.22-0.29 for normally consolidated samples tested at  $\sigma'_{vc}$  of 100, 200, 300, 400 and 500 kPa (i.e., all  $\sigma'_{vc}$  exceeded the in-situ preconsolidation stresses). The  $s_u/\sigma'_{vc}$  ratios from the FVTs and CPT range from about 0.4-0.5 at 6-8 m depth to about 0.3-0.4 at 14-18 m depth; the higher  $s_u/\sigma'_{vc}$  ratios at shallower depths may partly reflect the effects of light over-consolidation in situ, as discussed previously. The  $s_u/\sigma'_{vc}$  ratios from the FVTs and CPT are greater than from the DSS tests by an amount that cannot be explained by the small differences in overconsolidation ratio or by typical differences between the strengths obtained by these test types. For example, Bjerrum's (1973) empirical factor for correcting FVT strengths to "field" conditions, which are generally similar to DSS strengths, is greater than unity for this low PI soil and thus does not help explain the observed differences. Instead, a primary concern with the FVT and CPT data for this site is the potential for the thin sand interbeds to enhance local drainage and shear strength, which would bias the  $s_u/\sigma'_{vc}$  ratios unconservatively high. For example, CPT tip resistances in soft silts and clays are often about 2-3 times greater for drained penetration than undrained penetration, with partially drained penetration resulting in some intermediate degree of elevated penetration resistance (e.g., DeJong et al. 2012). The constant volume DSS tests have the advantage that they represent fully undrained conditions during testing and their shearing resistance would be relatively unaffected by thin, horizontal interbeds of sand. For the

purposes of this paper, it is assumed that the project site will be raised with fill materials such that the silt will become normally consolidated over its full thickness. Accordingly, the  $s_u/\sigma'_{vc}$  ratio is estimated to be about 0.27 for these conditions.

The selection of strengths for use in an NDA, and hence for the constitutive model calibration, needs to consider the effects of multi-directional shaking and higher strain rates during seismic loading. The cyclic undrained DSS tests were performed at a loading frequency of 0.1 Hz, whereas the dominant loading frequencies for this soft site during an earthquake would likely be about an order of magnitude greater (e.g., closer to 1 Hz). Accordingly, the cyclic strengths from the DSS tests could be increased by about 9% to represent the in-situ cyclic strengths during an earthquake (e.g., Boulanger & Idriss 2007). At the same time, cyclic strengths from two-directional loading tests are smaller than those from one-directional loading tests by about 4% for clay-like soils and about 10-20% for sand-like soils (e.g., Boulanger & Idriss 2007). Accordingly, the cyclic strengths obtained for FRD silt from the DSS tests might reasonably be reduced by 5-10% for the effects of two-directional shaking, given its intermediate plasticity characteristics. The effects of strain rate and multi-directional shaking are approximately equal and opposite for this particular set of data, such that  $s_u/\sigma'_{vc} = 0.27$  was also considered applicable for use in an NDA and hence constitutive model calibration.

### 3 PM4SILT BACKGROUND

The PM4Silt model is a critical state based and stress-ratio controlled bounding surface plasticity model developed for clays and plastic silts that exhibit stress-history normalized undrained shear strengths. The bounding and dilation stress ratios ( $M^b$  and  $M^d$ ) are functions of the state parameter ( $\xi$ ), such that they converge to the critical state stress ratio ( $M$ ) as the soil is sheared to critical state ( $\xi = 0$ ). The bounding surface relationship allows for separate adjustments for states that are loose or "wet" of critical state (i.e.,  $p' > p'_{cs}$ , where  $p'_{cs}$  is the mean effective stress at critical state for the current void ratio) and dense or "dry" of critical state (i.e.,  $p' < p'_{cs}$ ), as illustrated in Figure 1. The plastic modulus and dilatancy relationships are functions of a fabric tensor and its history. The model was formulated for approximating the engineering behaviors of primary concern for most earthquake engineering applications, which are: (1) monotonic undrained shear strength; (2) cyclic undrained shear strength and associated stress-strain responses; and (3) secant shear moduli and equivalent damping ratios. The model does not include a cap and therefore is not suited for simulating consolidation settlements under increasing overburden stresses or directly simulating strength evolution with consolidation stress history (e.g., increasing  $p'$  along constant stress ratio loading paths). The constitutive equations and details of the model are provided in the report by Boulanger & Ziotopoulou (2018).

The four primary input parameters are: undrained shear strength at critical state ( $s_{u,cs}$ ) or undrained shear strength ratio at critical state ( $s_{u,cs}/\sigma'_{vc}$ ), shear modulus coefficient ( $G_o$ ), contraction rate parameter ( $h_{po}$ ), and post-strong-shaking shear strength reduction factor ( $F_{su}$ ). The specified value for  $s_{u,cs}$  is used internally to position the critical state line at the time of model initialization, conditional on the other input parameters. The shear modulus coefficient should be selected to match the small-strain shear modulus ( $G_{max}$ ) corresponding to the measured or estimated in-situ  $V_s$ . The contraction rate parameter should be calibrated to approximate the expected cyclic strength curve [i.e., cyclic resistance ratio (CRR) versus number of uniform loading cycles to reach a specified failure criterion]. The post-strong-shaking shear strength reduction factor is used in simulations of boundary value problems and is not applicable to the calibration examples presented herein; the value of  $F_{su}$  should be selected based on the soil characteristics and the shear strains that develop in the system during strong shaking (Boulanger & Ziotopoulou 2018).

The model has twenty secondary input parameters for which default values were developed based on a generalized calibration to typical cyclic loading behaviors. Default values are embedded in the initialization section of the model code and are applied unless specified otherwise by the user. Nonetheless, there are several parameters that the user may adjust for improved soil-specific calibrations, as illustrated herein.

Table 1. Input parameters for PM4Silt.

Input parameter <sup>a</sup>	Default value	Fraser River Delta silt		
		Calibration No. 1	Calibration No. 2	Calibration No. 3
$s_{u,cs} - s_u$ at critical state	– <sup>b</sup>	0.27	0.27	0.27
$G_o$ – shear modulus coefficient	– <sup>b</sup>	500	$f(\sigma'_{vc})$ <sup>b</sup>	500
$h_{po}$ – contraction rate parameter	– <sup>b</sup>	2.5	3.0	25.0
$n_G$ – shear modulus exponent	0.75	0.6	1.0	0.6
$h_o$ – plastic modulus ratio	0.5	0.4	0.4	0.1
$e_o$ – initial void ratio	0.9	0.922	0.922	0.922
$\lambda$ – compressibility in $e-\ln(p')$ space	0.06	0.057	0.057	0.057
$\phi^{cs}_{cv}$ – critical state friction angle	32°	32°	32°	32°
$n^{b,wet}$ – bounding surface parameter	0.8	1.0	1.0	1.0
$n^{b,dry}$ – bounding surface parameter	0.5	– <sup>c</sup>	– <sup>c</sup>	– <sup>c</sup>
$n^d$ – dilation surface parameter	0.3	– <sup>c</sup>	– <sup>c</sup>	– <sup>c</sup>
$A_{do}$ – dilatancy parameter	0.8	– <sup>c</sup>	– <sup>c</sup>	– <sup>c</sup>
$r_{u,max}$ – sets bounding $p_{min}$	$p_{min} = p_{cs}/8$	0.95	0.95	0.95
$Z_{max}$ – fabric term	$10 \leq 40(s_u/\sigma'_{vc}) \leq 20$	– <sup>c</sup>	– <sup>c</sup>	– <sup>c</sup>
$C_z$ – fabric growth parameter	100	25	25	30
$C_e$ – strain accumulation rate factor	$0.5 \leq (1.2s_u/\sigma'_{vc} + 0.2) \leq 1.3$	0.2	0.2	0.25
$C_{GD}$ – modulus degradation factor	3.0	6.0	– <sup>c</sup>	– <sup>c</sup>
$C_{kaf}$ – plastic modulus factor	4.0	– <sup>c</sup>	– <sup>c</sup>	– <sup>c</sup>
$\nu_o$ – Poisson ratio	0.3	– <sup>c</sup>	– <sup>c</sup>	– <sup>c</sup>

<sup>a</sup> Excluding post-shaking analysis parameters ( $F_{su}$ , PostShake,  $C_{GC}$ ) and hour-glassing control parameters ( $cr_{hg}$ ,  $ch_g$ ).

<sup>b</sup> Required input parameter that does not have a default value.

<sup>c</sup> Retained default value.

<sup>d</sup> Function based on fit to the measured shear wave velocity profile.

The primary and secondary input parameters are listed in Table 1, along with the default values where applicable. Responses of the model for a baseline set of primary input parameters in combination with the default secondary parameters are provided in the report by Boulanger & Ziotopoulou (2018).

## 4 CALIBRATION OF PM4SILT FOR FRASER RIVER DELTA SILT

### 4.1 Calibration process

The process for calibrating PM4Silt is iterative, with the preferred sequence depending on the available information and the constitutive responses of primary interest. The process used for the present calibration requires that the user have a basic understanding of the model parameters and their influences as illustrated in Boulanger and Ziotopoulou (2018). The process can be summarized as follows:

1. select a value for the primary parameter  $s_{u,cs}/\sigma'_{vc}$  that describes the variation of  $s_u$  with depth in this silt deposit;
2. select values for the secondary parameters  $e_o$ ,  $\lambda$ , and  $\phi'_{cv}$  that can be based on the available laboratory test data;
3. select values for the primary parameter  $G_o$  and secondary parameter  $n_G$  that describe the variation of  $V_s$  with depth in this silt deposit;
4. assign a trial value to  $h_{po}$  to start the iterative calibration process;
5. simulate monotonic undrained DSS loading and use  $n^{b,wet}$  to adjust the peak  $s_u$  if the soil is initially wet of critical;
6. simulate cyclic undrained DSS loading at different strain amplitudes and use  $h_o$  to adjust, as desired, the dependence of secant shear moduli and equivalent damping ratios on cyclic shear strain amplitude;
7. simulate cyclic undrained DSS loading with uniform cyclic stress ratios and use  $h_{po}$  to adjust the fit to the cyclic DSS laboratory test data for CRR versus number of uniform loading cycles to cause a peak shear strain of 3%;
8. examine the stress-strain and stress-path responses of the above cyclic loading simulations, and use the secondary parameters  $C_z$ ,  $C_e$ ,  $C_{GD}$ ,  $r_{u,max}$ , and  $n_G$  to adjust the shear strain accumulation rate and other features of behavior; and
9. repeat steps [5] through [8] until no further revisions to input parameters are warranted.

#### 4.2 Alternative calibrations for FRD silt

Three alternative calibrations (i.e., sets of input parameters) were developed for FRD silt to illustrate the effects of emphasizing different behavioral considerations during calibration. Calibrations No. 1 and No. 2 illustrate the effect of alternative approaches to fitting the measured  $V_s$  profile. Calibration No. 3 illustrates the effect of placing greater emphasis on matching the stress-strain response from the monotonic undrained DSS tests, as opposed to matching empirical correlations for strain-dependent secant shear moduli and equivalent damping ratios. The input parameters for these three calibrations are listed in Table 1 and discussed below.

##### 4.2.1 Step [1]

The  $s_{u,cs}/\sigma'_{vc}$  was set to 0.27 for the full deposit based on the monotonic DSS test results, the expectation that the deposit will be nearly normally consolidated over its full thickness under the hypothetical future loading, and the previous discussion of strain rate and multi-directional shaking effects.

##### 4.2.2 Step [2]

The initial void ratio ( $e_o$ ) was set to 0.92, the slope of the critical state line ( $\lambda$ ) was set to 0.057, and the critical state friction angle ( $\phi'_{cv}$ ) was set to  $32^\circ$  for the full deposit based on the available laboratory test data, including the results from the index (e.g., water content), consolidation and DSS testing. A constant value of  $e_o$  was used for the full deposit because field data showed only modest variation with depth. The corresponding value for the saturated density was  $1.88 \text{ Mg/m}^3$ .

##### 4.2.3 Step [3]

Two alternative approaches were used to determine  $G_o$  and  $n_G$  values that fit the measured  $V_s$  profile shown in Figure 1. A fit to the  $V_s$  data between depths of 6 and 15 m in the FRD silt was first obtained as,

$$V_s = 151m/s \left( \frac{\sigma'_{vc}}{P_A} \right)^{0.30} \quad (1)$$

The corresponding relationship for the small-strain shear modulus ( $G_{\max}$ ), assuming the saturated density is a constant for the full deposit, can be expressed as,

$$G_{\max} = \rho(V_s)^2 = 421P_A \left( \frac{\sigma'_{vc}}{P_A} \right)^{0.60} \quad (2)$$

The relationship for  $G_{\max}$  in PM4Silt is based on the mean in-plane effective stress, which in turn depends on the coefficient of earth pressure at rest ( $K_o$ ):

$$G_{\max} = G_o P_A \left( \frac{\sigma'_{vc} \left( \frac{1+K_o}{2} \right)}{P_A} \right)^{n_G} \quad (3)$$

The first calibration approach (used for Calibrations No. 1 and No. 3) assumes  $K_o = 0.5$  throughout the deposit and sets  $n_G = 0.6$  based on the  $V_s$  data, leading to the relationship:

$$G_{\max} = 0.841 G_o P_A \left( \frac{\sigma'_{vc}}{P_A} \right)^{0.6} \quad (4)$$

This expression was matched to that based on the in-situ  $V_s$  data by setting  $G_o = 421/0.841 = 500$ .

The second calibration approach (used for Calibration No. 2) was to set  $n_G$  based on other considerations, and then have  $G_o$  vary with confining stress. This approach was also matched to that based on the in-situ  $V_s$  data by determining  $G_o$  as,

$$G_o = 500 \frac{\left( \frac{\sigma'_{vc} \left( \frac{1+K_o}{2} \right)}{P_A} \right)^{0.60}}{\left( \frac{\sigma'_{vc} \left( \frac{1+K_o}{2} \right)}{P_A} \right)^{n_G}} \quad (5)$$

The value of  $n_G$  for this second approach was eventually set to 1.0 during the iterative calibration process because it improved the simulation of stress-strain responses during cyclic undrained DSS loading, as discussed later. Accordingly, the value of  $G_o$  based on the above expression, and again assuming  $K_o = 0.5$ , ranged from 651 at a depth of 6.0 m (where  $\sigma'_{vc} = 70$  kPa) to 471 at a depth of 16 m (where  $\sigma'_{vc} = 157$  kPa).

The above two approaches to setting  $G_o$  and  $n_G$  provide identical fits to the  $G_{\max}$  profile computed from the in-situ  $V_s$  data, as illustrated in Figure 3, and are both easily implemented in a numerical model. The question arises, however, as to whether these alternative approaches to fitting the in-situ  $V_s$  data have a significant effect on other aspects of the constitutive model's calibration and performance. This question is addressed later by the comparison of results obtained using Calibrations No. 1 and No. 2, which otherwise are very similar.

#### 4.2.4 Steps [4-9]

Execution of the remaining steps [4-9] for FRD silt required deciding whether to put greater emphasis on matching: (1) the stress-strain response in monotonic undrained DSS loading; or (2) empirical relationships for secant shear moduli reduction and equivalent damping ratio versus cyclic shear strain amplitude. The monotonic stress-strain responses from the DSS tests imply an equivalent secant shear modulus reduction curve that is significantly different (shifted leftward) from the empirical relationships recommended by Vucetic & Dobry (1991). For this reason, it is impossible to develop a calibration that matches both of these behaviors/relationships, such that a choice must be made regarding which behavior/relationship should be given more weight. Calibrations No. 1 and No. 2 emphasize matching of the empirical relationships by Vucetic & Dobry (1991), whereas Calibration No. 3 emphasizes matching of the monotonic DSS tests.

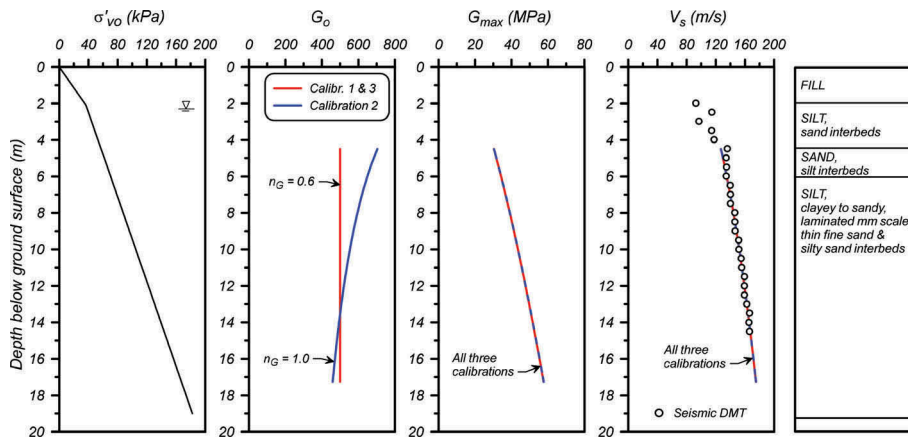


Figure 3. Alternative approaches for matching the in-situ small-strain shear modulus profile.

### 4.3 Comparison of simulation and laboratory test results

#### 4.3.1 Monotonic undrained DSS loading

The measured stress-strain and stress path responses from the monotonic undrained DSS tests and the first  $\frac{1}{4}$  cycle for each cyclic undrained DSS test are presented together in Figure 4. The responses from the first  $\frac{1}{4}$  cycle of loading from the cyclic DSS tests are equivalent to the first part of a monotonic loading test. Past studies have demonstrated that laboratory tests on field samples can significantly underestimate the initial stiffness of in-situ soils depending on the degree of sample disturbance, testing procedures and testing device (e.g., Lunne et al. 2006). The initial stiffness from these DSS tests shows significant variability, which likely reflects variations in each of these influencing factors. In addition, the initial stiffness from the cyclic DSS tests are generally greater than from the monotonic DSS tests, which may partly be due to the effects of increased strain rate (e.g., Matesic & Vucetic 2003). The monotonic DSS tests had  $\sigma'_{vc}$  of 100, 200, 300, 400, and 500 kPa, but the initial stiffness did not follow any clear pattern with regard to  $\sigma'_{vc}$ . For these reasons, greater weight was given to the stiffest responses obtained from these DSS tests.

The simulated responses for Calibrations No. 1 and No. 2 are almost identical and initially much stiffer than any equal of the DSS tests, as shown in Figure 4. The initially stiffer stress-strain responses in the simulations are a direct consequence of the decisions to: (1) base  $G_0$  on the in-situ  $V_s$  data and (2) calibrate the plastic modulus ratio ( $h_0$ ) to approximate the empirical relationship by Vucetic & Dobry (1991) for strain-dependent secant shear moduli and equivalent damping ratios, rather than attempting to match the monotonic DSS loading responses. The parameter  $n^{b,wet}$  was set to 1.0 for both calibrations because this limits the peak shear resistance to  $s_{u,cs}$  in the simulation, which better approximates the strain-hardening responses observed in the tests. Simulations were repeated for  $\sigma'_{vc}$  of 50-200 kPa, which spans the range of in-situ stresses for this deposit, to confirm that the normalized stress-strain and stress path responses are insensitive to  $\sigma'_{vc}$ .

The simulated response for Calibration No. 3, also shown in Figure 4, closely tracks the upper range of the initial stiffnesses from the DSS tests and is not as stiff as the other two calibrations. The smaller initial stiffness obtained with Calibration No. 3 is a direct consequence of reducing  $h_0$  to 0.1 (versus the 0.4 used for Calibrations No. 1 and No.2) to better approximate the upper range of the initial responses from these DSS tests.

#### 4.3.2 Shear modulus reduction and equivalent damping ratios

Normalized secant shear moduli ( $G/G_{max}$ ) and equivalent damping ratios from simulations of cyclic undrained DSS loading at  $\sigma'_{vc}$  of 100 and 200 kPa for Calibrations 1, 2 and 3 are

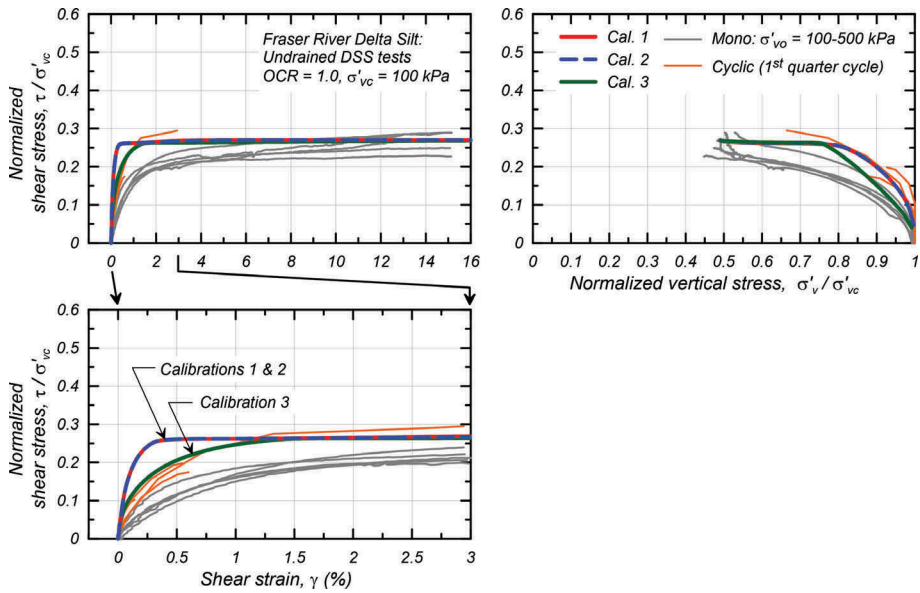


Figure 4. Measured and simulated responses to monotonic undrained DSS loading.

compared to the empirical curves by Vucetic & Dobry (1991) for  $PI = 0$  and 15 fine-grained soils in Figure 5. The stress-strain responses from these simulations are compared in Figure 6. The simulations have three cycles of loading at each strain amplitude; the secant shear modulus and damping ratio from the last cycle at each strain amplitude are the values plotted in Figure 5. These simulations use  $K_o = 1.0$ , as this better represents the experimental conditions upon which the empirical correlations are largely based.

The parameter  $h_o$  was reduced to 0.4 (from the default value of 0.5) for Calibrations No. 1 and No. 2 to produce simulated  $G/G_{max}$  ratios that are intermediate to the empirical  $PI = 0$  and 15 curves for cyclic strain amplitudes less than about 0.1%. The more rapid drop in  $G/G_{max}$  and increase in damping ratios (relative to the empirical  $PI = 0$  and 15 curves) as cyclic strain amplitudes exceed about 0.1% reflect increased cyclic degradation for this soft soil condition. This deviation from the empirical curves at larger strains is considered reasonable for these soft soil conditions, and thus no attempt was made to improve the fit with the empirical curves at these larger strains. Calibrations No. 1 and No. 2 produce almost identical stress-strain responses (Figure 6) and almost identical  $G/G_{max}$  and equivalent damping ratios (Figure 5), with only minor differences developing at the largest cyclic shear strain amplitudes. The simulated responses are almost identical because the two calibrations have the same  $G_{max}$ ,  $S_{u,cs}$  and  $h_o$  values, which collectively have the strongest effect on stress-strain responses at cyclic shear strain amplitudes less than about 0.5%. This combination of parameters is the reason the simulations of monotonic undrained DSS loading are much stiffer than the experimental data (Figure 4), as discussed in the previous section.

The parameter  $h_o$  was reduced to 0.1 for Calibration No. 3 to better approximate the monotonic undrained DSS tests (Figure 4), which resulted in the simulated  $G/G_{max}$  ratios being shifted left of the empirical  $PI = 0$  and 15 curves (Figure 5). Smaller  $G/G_{max}$  ratios and larger damping ratios (relative to the empirical  $PI = 0$  and 15 curves) develop over a wide range of cyclic strain amplitudes. Calibration No. 3 produces stress-strain loops (Figure 6) with less cyclic degradation at a shear strain amplitude of 0.3% than the other two calibrations. Cyclic degradation at this strain amplitude is less for Calibration No. 3 because its smaller shear stiffness results in smaller peak shear stress ratios, which slowed the generation of plastic volumetric strains and hence excess pore water pressure.

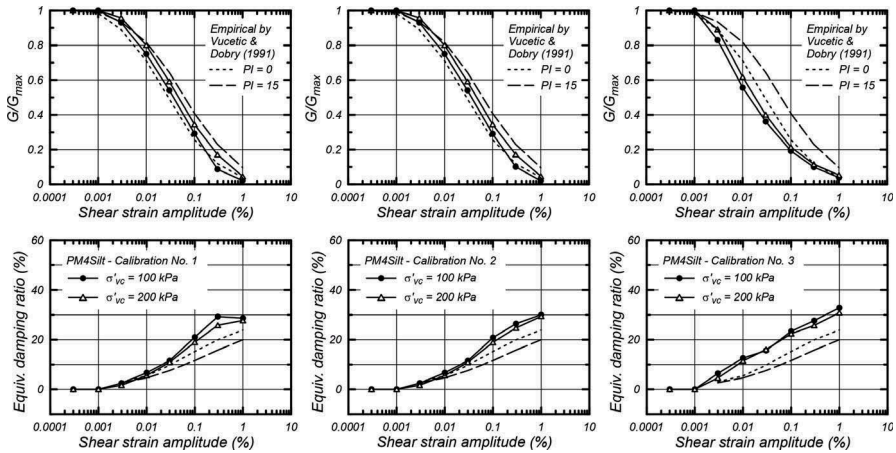


Figure 5. Shear modulus reduction and equivalent damping ratios versus cyclic shear strain amplitude for undrained DSS loading: Simulation results for the 3<sup>rd</sup> loading cycle with Calibrations 1, 2, and 3 compared with the empirical relationships by Vucetic & Dobry (1991).

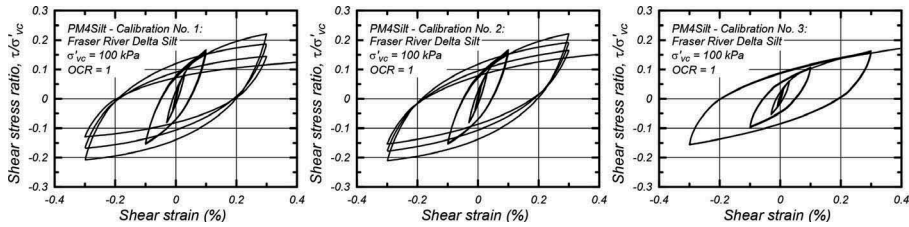


Figure 6. Simulated stress responses for undrained DSS loading at different cyclic shear strain amplitudes with Calibrations 1, 2 and 3.

#### 4.3.3 Cyclic undrained DSS loading

Simulated cyclic strength curves for Calibrations 1, 2, and 3 are compared to the measured cyclic DSS strengths in Figure 7. The cyclic DSS tests were performed with  $\sigma'_{vc} = 100$  kPa, whereas simulation results are presented for  $\sigma'_{vc} = 100$  kPa and 200 kPa to evaluate the simulated effect of increasing consolidation stress. The simulations used  $K_o = 0.5$  and the cyclic strengths are plotted for a peak single amplitude shear strain of 3%. Note that the DSS test at CSR = 0.29 is plotted at  $\frac{1}{2}$  cycle, rather than at  $\frac{1}{4}$  or  $\frac{3}{4}$  cycle as might be expected, due to an interesting detail of its response; this sample reached a shear strain of 2.9% when the shear stress reached its peak value at  $\frac{1}{4}$  cycle, reached almost exactly 3.0% strain while the shear stress was decreasing (but was still positive), and then exceeded 3% shear strain in the opposite direction at  $\frac{3}{4}$  cycle. Describing the loading with anything more refined than  $\frac{1}{4}$  cycle increments implies more accuracy than is justified, so  $\frac{1}{2}$  cycle was used for plotting this particular test. For the simulations, the parameter  $h_{po}$  was iteratively adjusted to bring the simulated cyclic strength curve into an average agreement with the cyclic DSS test results for  $\sigma'_{vc} = 100$  kPa; adjusting  $h_{po}$  has a stronger effect on the cyclic strength curve at larger numbers of loading cycles because the simulated cyclic strength is always approximately equal to the peak  $s_u/\sigma'_{vc}$  ratio near a single loading cycle. Calibrations No. 1 and No. 2 produced similar cyclic strength curves, both of which are slightly steeper than the measured cyclic strength data. Calibration No. 3 produced a flatter cyclic strength curve that is in better agreement with the measured cyclic strength data. All three calibrations produce cyclic strengths that decrease slightly with increasing  $\sigma'_{vc}$ ; the relative magnitude of the

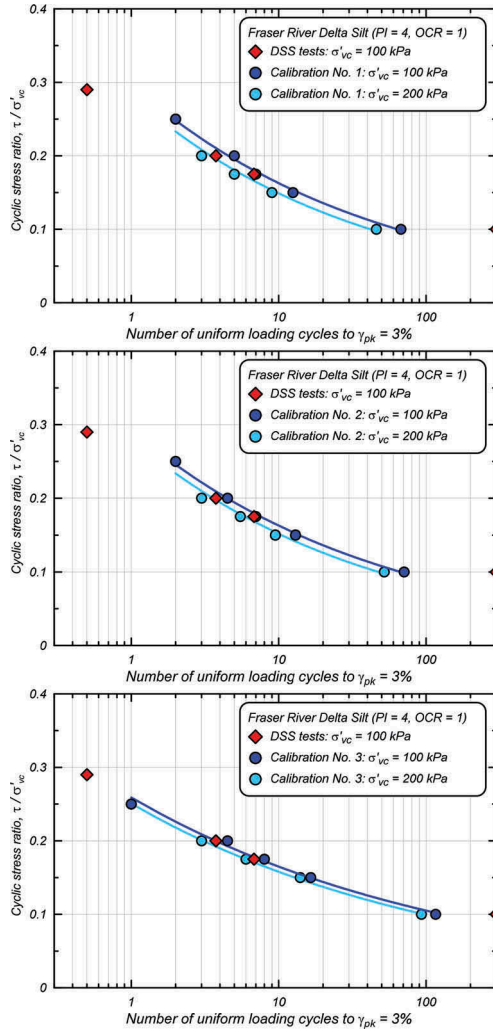


Figure 7. Cyclic stress ratio versus number of uniform loading cycles to a peak shear strain of 3% in cyclic undrained DSS loading: Simulation results for Calibrations 1, 2 and 3.

decrease in cyclic strength is more than expected for a clay-like soil and less than expected for a sand-like soil, which seems reasonable for this low-plasticity silt.

Simulated stress-strain and stress-path responses for Calibrations 1, 2 and 3 are compared with measured responses for specimens loaded at CSRs of about 0.175, 0.20, and 0.25 in Figures 8, 9 and 10, respectively. For all calibrations,  $r_{u,max}$  was set to 0.95 based on the measured pore pressure responses, and the values for  $C_z$  and  $C_\varepsilon$  were reduced to 25-30 (compared to a default value of 100) and 0.20-0.25 (compared to a default value of 0.5), respectively to reduce the rates of shear strain accumulation in the simulations to levels consistent with the measured responses at different loading levels. Note that  $C_z$  was used to adjust the rate of strain accumulation in the range of 1-3% shear strain as the fabric tensor is first growing, and  $C_\varepsilon$  was used to adjust strain rate accumulation at larger shear strains. For Calibration No. 1 (with  $n_G = 0.6$ ), the shear modulus degradation parameter  $C_{GD}$  was increased to 6.0 (compared to the default value of 3.0) to improve the shape of the stress-strain hysteresis loops at shear strains ranging from 3 to 10%. In particular, increasing  $C_{GD}$  helped produce the slow and steady rate at which the shear stress

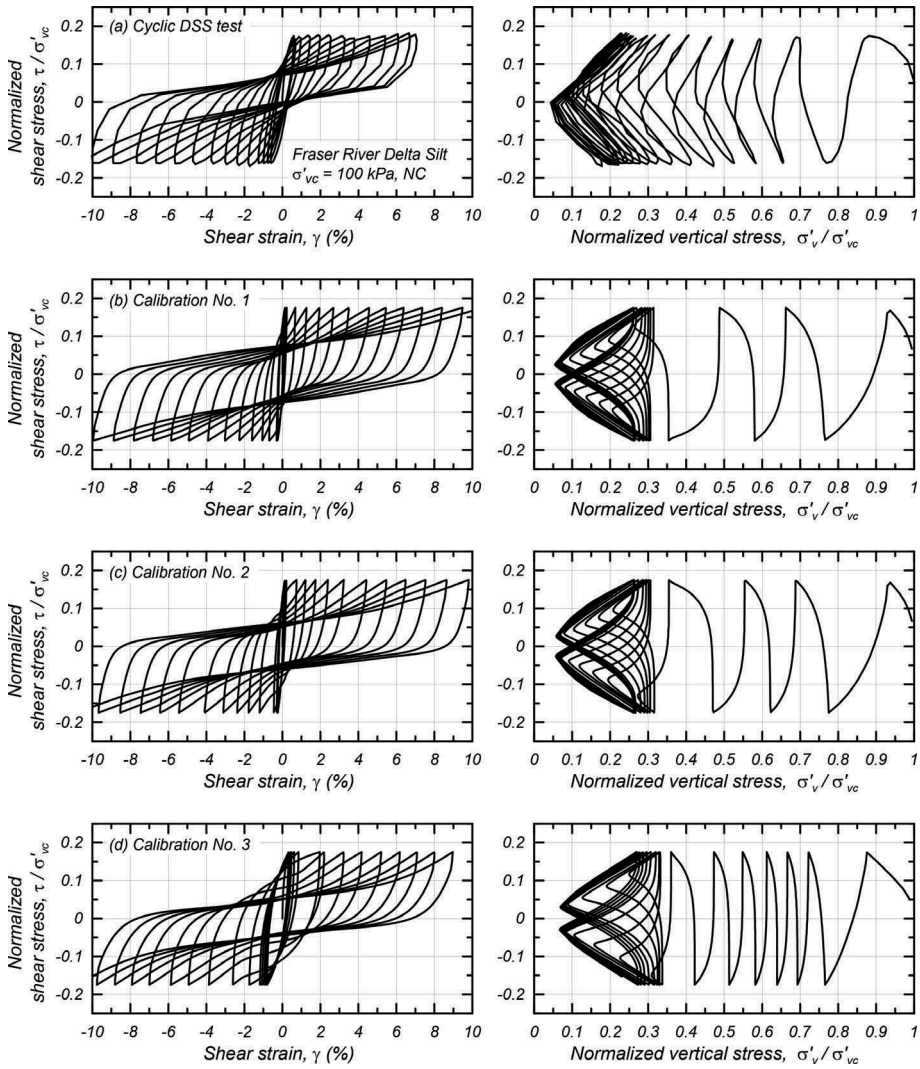


Figure 8. Stress-strain and stress path responses for cyclic undrained DSS loading at CSR = 0.175: (a) measured, (b) Calibration No. 1, (c) Calibration No. 2, and (d) Calibration No. 3.

increases during loading after a shear stress reversal (i.e., after  $r_u$  transiently reaches its maximum value). For Calibration No. 2 (with  $n_G = 1.0$ ), the parameter  $C_{GD}$  was left at its default value because the simulations of the stress-strain hysteresis loops at larger shear strains was already superior to that for Calibration No. 1. In particular, the use of a larger  $n_G$  value causes the elastic shear and bulk moduli to reduce by greater amounts when  $r_u$  is near its maximum value, which resulted in better simulations of the pinched (narrow) hysteresis loops. The improvement in simulations obtained by increasing  $n_G$  to 1.0 does not necessarily mean that this parameter provides a better description of how elastic moduli vary with  $p'$ , but rather may reflect compensating effects of approximations in all the other constitutive modeling components (e.g., plastic modulus, dilatancy, fabric). For Calibration No. 3 (with  $n_G = 0.6$ ), the more rapid reduction in secant shear modulus provided by having reduced  $h_o$  to 0.1 resulted in good simulations of the pinched (narrow) hysteresis loops at larger shear strains, although the hysteresis loops for the first cycle to exceed shear strains of about 1% are wider than observed experimentally.

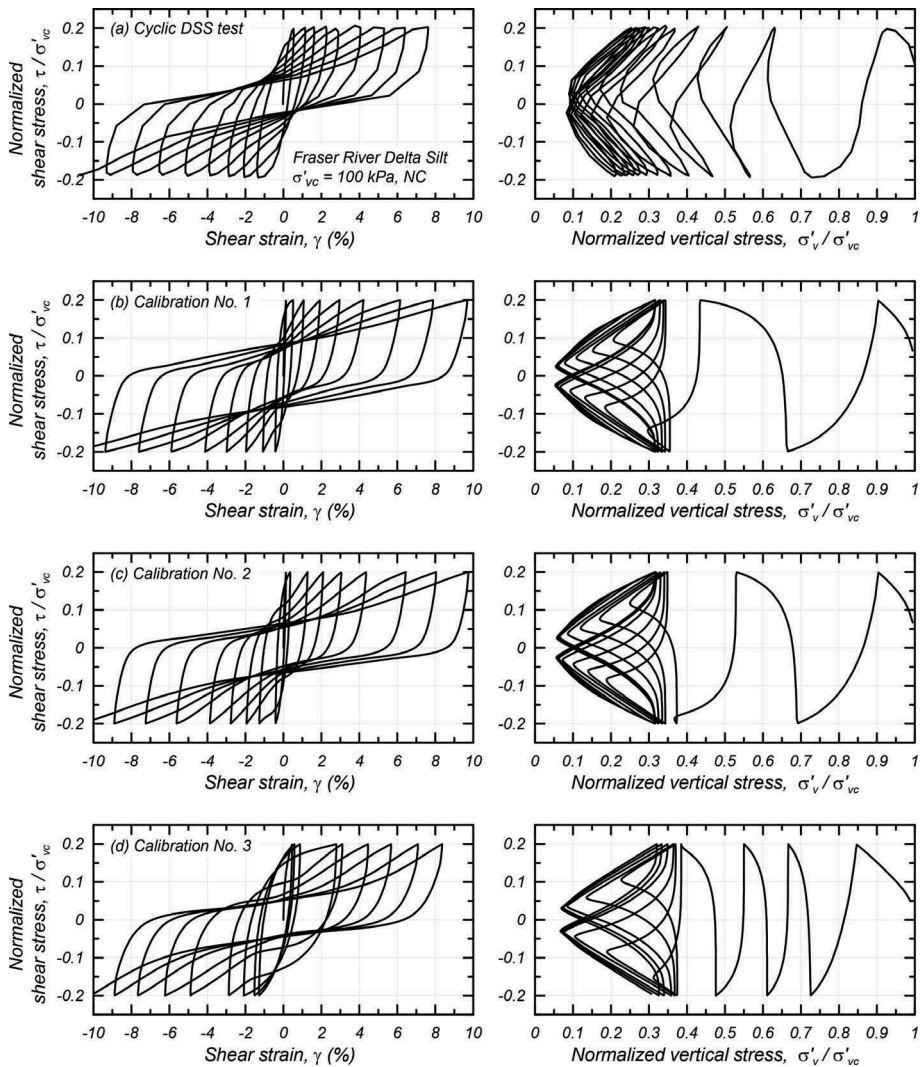


Figure 9. Stress-strain and stress path responses for cyclic undrained DSS loading at CSR = 0.20: (a) measured, (b) Calibration No. 1, (c) Calibration No. 2, and (d) Calibration No. 3.

The simulations and test data for the specimens loaded at CSRs of about 0.175 and 0.20, as shown in Figures 8 and 9, are further compared in Figures 11a and 11b in terms of  $r_u$  versus normalized number of loading cycles ( $N/N_{\gamma=3\%}$ ). The simulations using Calibrations No. 1 and No. 2 predicted faster rates of pore pressure generation than were measured in these tests, whereas the simulations using Calibration No. 3 were in reasonably good agreement with the measured responses. These differences in pore pressure generation rates are also evident in how the different stress paths evolved with each loading cycle (i.e., Figures 8 and 9), since  $r_u$  is equal to  $1 - \sigma'_v / \sigma'_{vc}$ .

#### 4.3.4 Discussion

Calibrations No. 1 and No. 2 produced comparable responses in almost all regards, including similar responses to monotonic undrained DSS loading, similar strain-dependent secant shear moduli and equivalent damping ratios, and similar cyclic strength curves and cyclic stress-strain responses. The cyclic stress-strain responses for Calibration No. 2 provided a slightly

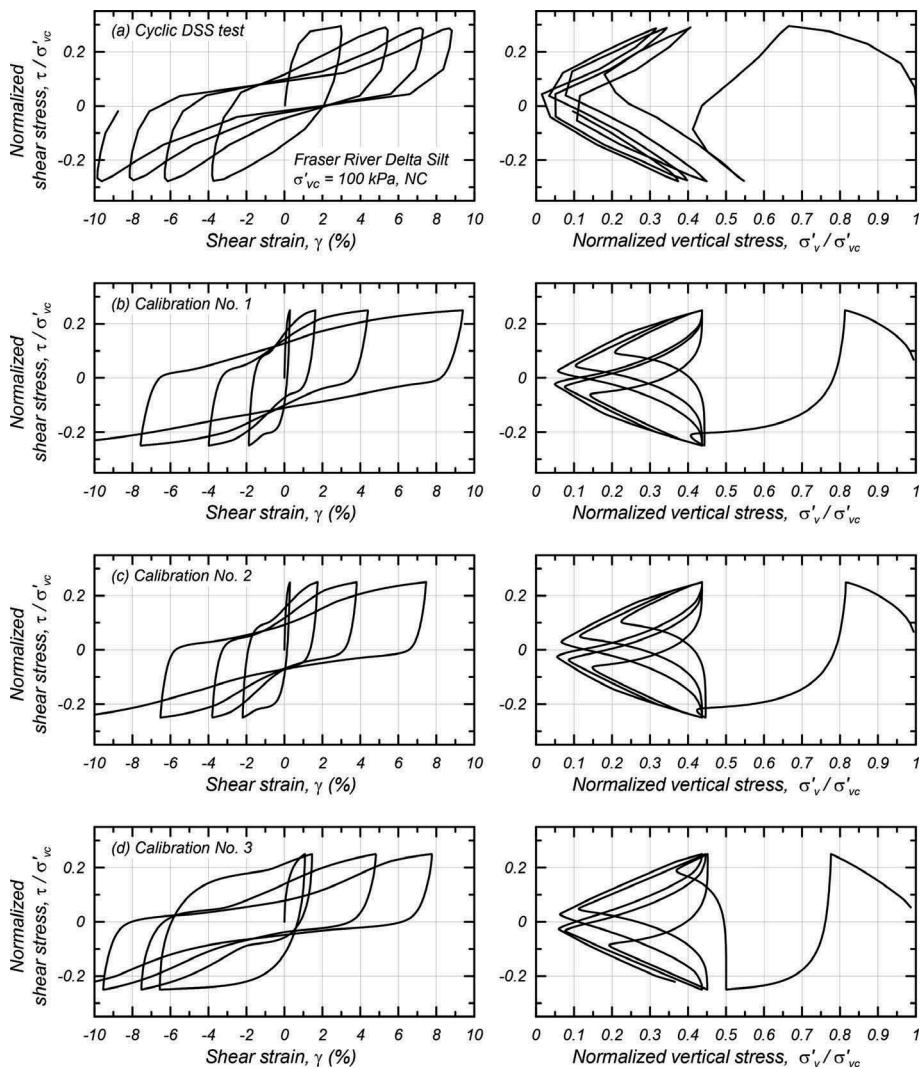


Figure 10. Stress-strain and stress path responses for cyclic undrained DSS loading at  $CSR \approx 0.25$ : (a) measured, (b) Calibration No. 1, (c) Calibration No. 2, and (d) Calibration No. 3.

improved approximation of the measured cyclic stress-strain responses, but the differences are unlikely to be of practical significance for most applications. The similarity in responses obtained using these two calibrations is not surprising given they targeted the same monotonic strengths, same cyclic strength curves, and same empirical  $G/G_{max}$  and equivalent damping ratio relationships, even though they used different means to approximate the in-situ  $V_s$  profile.

Calibration No. 3 provided better approximations of the stress-strain responses for monotonic and cyclic undrained DSS loading and a better fit (slope) for the cyclic strength curve, but produced smaller  $G/G_{max}$  ratios and greater equivalent damping ratios than expected based on the empirical correlations by Vucetic & Dobry (1991). Calibration No. 3 was based on the stiffest initial responses in the monotonic and cyclic DSS tests, which arguably reduces any potential bias toward lower stiffness caused by sample disturbance or other factors.

Any preference for Calibration No. 3 versus either Calibration No. 1 or No. 2 depends on the relative confidence that one places on the stiffness measurements from the DSS tests

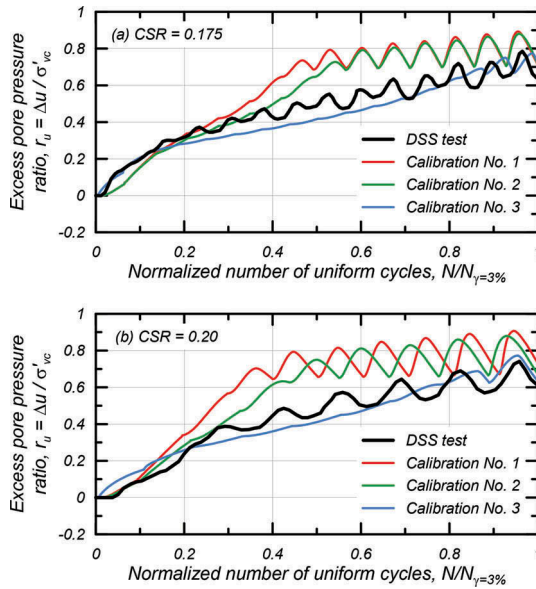


Figure 11. Measured and simulated excess pore pressure ratio versus normalized number of uniform loading cycles for cyclic undrained DSS loading at: (a) CSR = 0.175, and (b) CSR = 0.20.

versus the applicability of the empirical  $G/G_{\max}$  correlations. The tendency for DSS tests to underestimate secant shear moduli at smaller shear strains was evident in these test data, although this concern was partly alleviated by basing Calibration No. 3 on the stiffest initial responses. The empirical  $G/G_{\max}$  correlations have the advantage that they are generally based on data from dynamic/cyclic laboratory tests designed to measure small-strain properties (e.g., resonant column tests), but there is uncertainty in the application of any correlation to a specific soil. For the present dataset, these alternative calibrations are considered equally defensible and thus might reasonably be assigned equal confidences (or weights) if this aspect of modeling uncertainty was to be formally evaluated. For other soils or datasets, greater weight might be given to a calibration obtained by either approach depending on sample quality, testing procedures, data quality, soil type, and other factors.

All three calibrations are reasonable alternatives for use in NDA studies given the uncertainties involved in other aspects of any seismic performance evaluation (e.g., Boulanger & Ziotopoulou 2018). The differences between the three calibrations can be viewed as representing a component of constitutive modeling uncertainty, as noted above, but these differences are likely to be smaller than would be obtained if a second constitutive model was used for approximating these behaviors and subsequently used in evaluating the effects of constitutive modeling uncertainty.

## 5 CONCLUDING REMARKS

Three alternative calibrations of the PM4Silt constitutive model (Boulanger & Ziotopoulou 2018) were presented for a natural deposit of soft, normally consolidated to lightly over-consolidated, low-plasticity Fraser River Delta silt (ML) with a plasticity index of about 4. The site was characterized using cone penetration tests, seismic dilatometer tests, rotary wash borings, field vane shear tests, and advanced laboratory testing of thin-walled tube samples. Calibration of the PM4Silt model, which was developed for representing clays and plastic silts in geotechnical earthquake engineering applications, focused on approximating: (1) the monotonic undrained DSS strengths and stress-strain responses; (2) the cyclic undrained DSS

strengths and stress-strain responses; and (3) the strain-dependence of the secant shear moduli and equivalent damping ratios.

Calibrations No. 1 and No. 2 differed in how they approximated the in-situ  $V_s$  profile, but otherwise were calibrated to similar target responses, including the same empirical correlation for the strain-dependent secant shear moduli and equivalent damping ratios. The simulated responses for these two calibrations were similar in almost all regards.

Calibration No. 3 focused on approximating the monotonic and cyclic undrained DSS tests, at the expense of deviating from the empirical correlations for strain-dependent secant shear moduli and equivalent damping ratios. This calibration produced better agreement with the DSS test results, but the potential for the secant shear moduli from these tests to have been adversely affected by sample disturbance needs to be considered.

All three calibrations are considered reasonable alternatives for use in NDA studies, given the uncertainties involved in other aspects of any seismic performance evaluation. The results of this calibration study illustrate that PM4Silt is capable of reasonably approximating the range of monotonic and cyclic loading behaviors important to many earthquake engineering applications and is relatively easy to calibrate.

## ACKNOWLEDGMENTS

The constitutive modeling work presented herein was derived from studies supported by the National Science Foundation (grants CMMI-1300518 and CMMI-1635398) and the California Department of Water Resources (DWR) under Contract 4600009751. The laboratory testing program was supported by the Natural Sciences and Engineering Research Council of Canada (NSERC). The field testing was supported by the British Columbia Geological Survey, the City of Richmond, and the Joint Emergency Preparedness Program. Any opinions, findings, or recommendations expressed in this material are those of the authors and should not be interpreted as necessarily representing the official policies, either expressed or implied, of any of the above organizations. The authors also appreciate the assistance and contributions of Drs. Maria Sanin and Patrick Mohahan and Messrs. Harald Schremp, Bill Leung, Scott Jackson, and John Wong with various aspects of the field and laboratory testing studies and the helpful review comments provided by Professor Katerina Ziotopoulou and Mr. Viji Fernando.

## REFERENCES

- Amer, M. I., Kovacs, W. D., & Aggour, M. S. 1987. Cyclic simple shear size effects. *Journal of Geotechnical Engineering*, ASCE, 113(7),693-707, 10.1061/(ASCE)0733-9410(1987)113:7(693).
- Bjerrum, L. 1973. Problems of soil mechanics and construction on soft clays. *Proc., 8<sup>th</sup> International Conference on Soil Mechanics and Foundation Engineering*, Vol 3, 111-159.
- Boulanger, R. W., & Beaty, M. H. 2016. Seismic deformation analyses of embankment dams: A reviewer's checklist. *Proceedings, Celebrating the Value of Dams and Levees – Yesterday, Today and Tomorrow, 36th USSD Annual Meeting and Conference*, United States Society on Dams, Denver, CO, 535-546.
- Boulanger, R. W., & Idriss, I. M. 2007. Evaluation of cyclic softening in silts and clays. *Journal of Geotechnical and Geoenvironmental Engineering*, ASCE, 133(6),641-652, 10.1061/(ASCE)1090-0241(2007)133:6(641).
- Boulanger, R. W., & Ziotopoulou, K. 2017. *PM4Sand (Version 3.1): A sand plasticity model for earthquake engineering applications*. Report No. UCD/CGM-17/01, Center for Geotechnical Modeling, Department of Civil and Environmental Engineering, University of California, Davis, CA, 113 pp.
- Boulanger, R. W., & Ziotopoulou, K. 2018a. *PM4Silt (Version 1): A silt plasticity model for earthquake engineering applications*. Report No. UCD/CGM-18/01, Center for Geotechnical Modeling, Department of Civil and Environmental Engineering, University of California, Davis, CA.
- Boulanger, R. W., & Ziotopoulou, K. 2018b. On NDA practices for evaluating liquefaction effects. *Proc., Geotechnical Earthquake Engineering and Soil Dynamics V*, Geotechnical Special Publication 290, S. J. Brandenberg and M. T. Manzari, eds., ASCE, 1-20.

- Carlton, B. D., & Pestana, J. M. 2012. Small strain shear modulus of high and low plasticity clays and silts. *Proc., 15th World conference on earthquake engineering*, Lisbon, Portugal.
- DeJong, J. T., Jaeger, R. A., Randolph, M. F., Boulanger, R. W., & Wahl, D. 2012. Variable penetration rate cone testing for characterization of intermediate soils. *Geotechnical and Geophysical Site Characterization 4 (ISC'4)*, Coutinho and Mayne, eds., Taylor and Francis Group, London, 25-42.
- Itasca 2016. *FLAC, Fast Lagrangian Analysis of Continua*, User's Guide, Version 8.0. Itasca Consulting Group, Inc., Minneapolis, MN.
- Lunne, T., Berre, T., Andersen, K. H., Strandvik, S., & Sjørusen, M. 2006. Effects of sample disturbance and consolidation procedures on measured shear strength of soft marine Norwegian clays. *Canadian Geotechnical Journal*, 43: 726-750.
- Matesic, L., & Vucetic, M. 2003. Strain-rate effect on soil secant shear modulus at small cyclic strains. *Journal of Geotechnical and Geoenvironmental Engineering*, ASCE, 129(6): 536-549, 10.1061/(ASCE)1090-0241(2003)129:6(536).
- Price, A. B., Boulanger, R. W., DeJong, J. T., Parra Bastidas, A. M., & . Cyclic strengths and simulated CPT penetration resistances in intermediate soils. *6<sup>th</sup> International Conference on Earthquake Geotechnical Engineering*, November 1-4, Christchurch, New Zealand.
- Price, A. B., DeJong, J. T., & Boulanger, R. W. 2017. Cyclic loading response of silt with multiple loading events. *Journal of Geotechnical and Geoenvironmental Engineering*, ASCE, 143 (10):04017080, 10.1061/(ASCE)GT.1943-5606.0001759.
- Sanin, M. V., & Wijewickreme, D. 2006. Cyclic shear response of channel-fill Fraser River Delta silt. *Soil Dynamics and Earthquake Engineering*, 26(2006): 854-960, doi:10.1016/j.soildyn.2005.12.006.
- Vucetic, M., & Dobry, R. 1991. Effect of soil plasticity on cyclic response. *Journal of Geotechnical Engineering*, 117(1),89-107.
- Wijewickreme, D., & Sanin, M. V. 2008. Cyclic shear response of undisturbed and reconstituted low-plastic Fraser River silt. *Proc., Geotechnical Earthquake Engineering and Soil Dynamics IV*, GSP 181, ASCE.
- Ziotopoulou, K., & Boulanger, R. W. 2016. Plasticity modeling of liquefaction effects under sloping ground and irregular cyclic loading conditions. *Soil Dynamics and Earthquake Engineering*, 84 (2016), 269-283, 10.1016/j.soildyn.2016.02.013.